

## Article

# Flexible Electricity Dispatch of an Integrated Solar Combined Cycle through Thermal Energy Storage and Hydrogen Production

Miguel Ángel Reyes-Belmonte <sup>\*</sup>, Alejandra Ambrona-Bermúdez and Daniel Calvo-Blázquez

Department of Chemical and Energy Technology, School of Experimental Sciences and Technology (ESCET), Rey Juan Carlos University, 28933 Móstoles, Madrid, Spain; a.ambrona.2016@alumnos.urjc.es (A.A.-B.); d.calvob.2016@alumnos.urjc.es (D.C.-B.)

\* Correspondence: miguelangel.reyes@urjc.es

**Abstract:** In this work, the flexible operation of an Integrated Solar Combined Cycle (ISCC) power plant has been optimized considering two different energy storage approaches. The objective of this proposal is to meet variable users' grid demand for an extended period at the lowest cost of electricity. Medium temperature thermal energy storage (TES) and hydrogen generation configurations have been analyzed from a techno-economic point of view. Results found from annual solar plant performance indicate that molten salts storage solution is preferable based on the lower levelized cost of electricity (0.122 USD/kWh compared to 0.158 USD/kWh from the hydrogen generation case) due to the lower conversion efficiencies of hydrogen plant components. However, the hydrogen plant configuration exceeded, in terms of plant availability and grid demand coverage, as fewer design constraints resulted in a total demand coverage of 2155 h per year. It was also found that grid demand curves from industrial countries limit the deployment of medium-temperature TES systems coupled to ISCC power plants, since their typical demand curves are characterized by lower power demand around solar noon when solar radiation is higher. In such scenarios, the Brayton turbine design is constrained by noon grid demand, which limits the solar field and receiver thermal power design.

**Keywords:** Integrated Solar Combined Cycle; flexible dispatch; concentrating solar power; hydrogen production; modelling; energy storage



**Citation:** Reyes-Belmonte, M.Á.; Ambrona-Bermúdez, A.; Calvo-Blázquez, D. Flexible Electricity Dispatch of an Integrated Solar Combined Cycle through Thermal Energy Storage and Hydrogen Production. *Thermo* **2021**, *1*, 106–121. <https://doi.org/10.3390/thermo1010008>

Academic Editor: Johan Jacquemin

Received: 12 April 2021

Accepted: 2 June 2021

Published: 8 June 2021

**Publisher's Note:** MDPI stays neutral with regard to jurisdictional claims in published maps and institutional affiliations.



**Copyright:** © 2021 by the authors. Licensee MDPI, Basel, Switzerland. This article is an open access article distributed under the terms and conditions of the Creative Commons Attribution (CC BY) license (<https://creativecommons.org/licenses/by/4.0/>).

## 1. Introduction

Worldwide energy consumption is tightly connected to industrial and societal development [1]. Despite global efforts on energy-saving policies and more efficient systems, the reality shows that global energy consumption (whether as heat or electricity) is experiencing an annual growth to meet our living standards and countries' economic growth [2]. In many cases, the energy consumption growth has been achieved through an increase in fossil fuel consumption, whether for lower conversion costs or easier availability in meeting users' energy demands. This strong fossil fuel dependency has an undeniable impact on the environment based on their pollutant and greenhouse gases emissions, which are leading climate change. To reverse this situation, most countries have agreed through different platforms to reduce their emissions levels and to increase the contribution of renewable energy sources to the big picture. Examples include the Paris Climate Agreement, COP21, the United Nations Sustainable Development Goals and Europe's 2030 energy plan [3]. Despite the substantial efforts in renewable energy research, there are many areas for improvement that will pave the way towards a fully renewable energy scenario. In this manuscript, the topic has been addressed within solar thermal energy applications as this technology has shown a bright future and a fast cost reduction in the short term [4]. Among those challenges, increasing conversion efficiencies, reducing material costs and improving dispatchability are seen as the cornerstones for renewable energy technology deployment [5,6].

Regarding conversion efficiency enhancement, this aspect is crucial for the deployment of the technology as it means a direct impact on the levelized cost of electricity (LCoE). In the case of thermal energy conversion pathways, as in the case of concentrating solar power, this can be achieved whether by increasing working fluid temperature as stated in thermodynamics, by moving towards more efficient power cycles or by hybridizing with other renewable energy technologies [7]. For the first case, several proposals have been posed regarding high-temperature fluids for CSP applications such as using liquid metals [8,9], air [10,11] or inert particles [12,13]. Such options will enhance the current technology and material limits imposed by commercial molten salts [14]. Regarding more efficient power cycles, two major solutions have been proposed up to now, which can exceed 50% conversion efficiency. This efficiency target has been envisioned as one of the cornerstones for CSP technology deployment. On the one hand, supercritical CO<sub>2</sub> power cycle arrangements [15] have claimed great potential for CSP applications [16–18]. Despite the very promising results, the ongoing demonstration projects [19–21] and great expectations of sCO<sub>2</sub> power, up to now, combined cycle power plants are the only mature technology that has proven the highest conversion efficiency. Under both constraints, the Integrated Solar Combined Cycle (ISCC) approach seems to be the optimum solution. On the contrary, its high operating temperature draws a new challenge related to the energy storage for this configuration. In literature, several proposals have been posed to address plant layout configurations of ISCC and its energy storage due to the non-dispatchable external heat addition to the cycle [22–24]. Among the existing proposals, parabolic trough technologies supported by fired gas turbine cycle have been widely analyzed for steam generation at the bottoming Rankine cycle due to the technology's easier implementation and its lower cost [25]. These proposals also include plant layouts including thermal energy storage for extending solar field capacity [26], without thermal storage for LCoE reduction but at higher natural gas consumption [27] or for direct steam generation [28]. However, to acclaim for fully renewable configuration, some recent works proposed unfired gas turbine integration for ISCC, requiring the design of solar air receivers, the use of alternative heat transfer fluids [29,30] or its hybridization with other energy sources [31]. In those cases, the high temperatures achieved at the solar receiver limits thermal energy storage solutions and materials selection.

In this manuscript, two different energy storage proposals are integrated within an ISCC power cycle to increase electricity dispatch flexibility. Energy storage systems have been designed to meet the grid demand curve instantaneously during daylight hours so production can be extended in the evening to cover the peak demand. On the one hand, the exceeding thermal energy from the topping cycle can be used to heat molten salts that are later recovered when needed to increase the steam generation of the Rankine cycle and satisfy grid demand only with steam cycle operation. On the other hand, exceeding electricity generation from the ISCC can be used to run an alkaline electrolyzer to produce and store hydrogen that will be later converted into electricity using a phosphoric acid fuel cell when needed.

This paper's structure is organized as follows. In Section 2, the plant layout and working conditions for both energy storage proposals are presented. In Section 3, the flexible dispatch strategy is discussed, and instantaneous operative curves are described. In Section 4, ISCC annual performance under flexible operation strategy is analyzed and the levelized cost of electricity (LCoE) is estimated.

## 2. Materials and Methods

The general ISCC layout consists of an un-fired open Brayton cycle that receives its thermal energy through a solar air receiver fed from a north solar field. Energy from gas turbine exhaust is recovered through a heat recovery steam generator (HRSG) to run a Rankine bottoming cycle. As it can be observed in Figure 1, red lines represent hot air circulation along the Brayton cycle while blue lines indicate water/steam along the Rankine cycle. To provide enough dispatchability to the ISCC plant concept, two

independent energy storage approaches are proposed. On the one hand, Approach A (represented in the ocher box) is based on storing excess thermal energy from the topping cycle into molten salts using a dedicated heat exchanger. That energy will later be recovered on demand for additional steam generation to meet users' grid demand. On the other hand, Approach B (represented in green) is intended to produce hydrogen using surplus electricity in an electrolyzer. When needed, the stored hydrogen will be recovered in a fuel cell to produce electricity according to users' grid demand. The solar power plant located in Ouarzazate, Morocco (30.9° N, 6.93° W), has been chosen due to the strategic importance of recent CSP projects in the region.

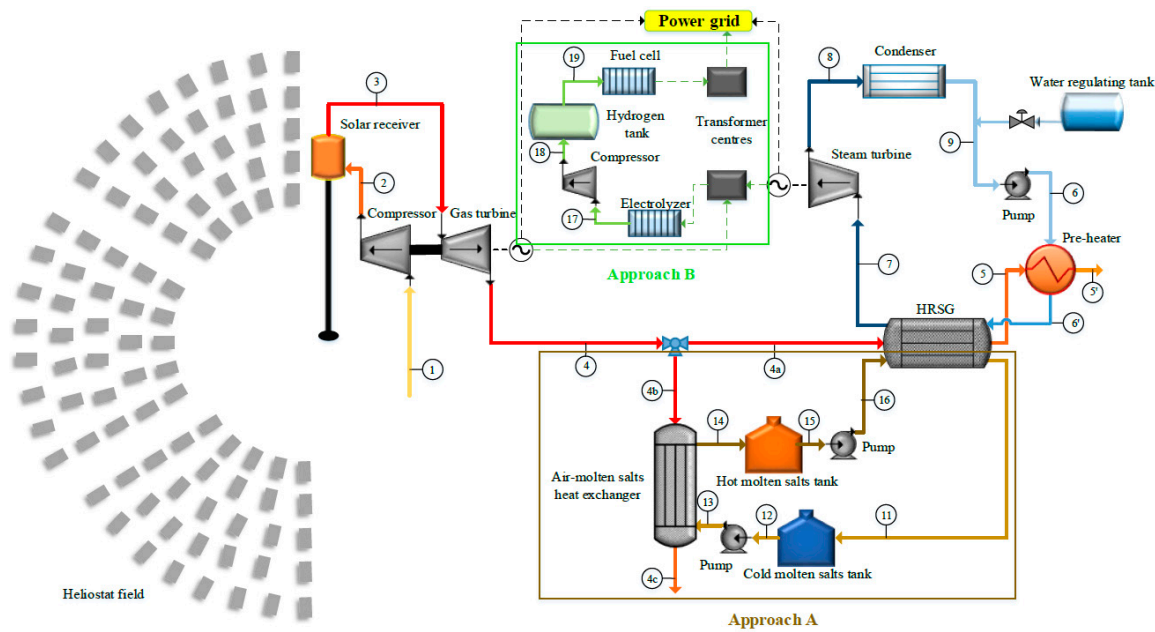


Figure 1. Integrated Solar Combined Cycle (ISCC) power plant layout coupled to two different energy storage approaches.

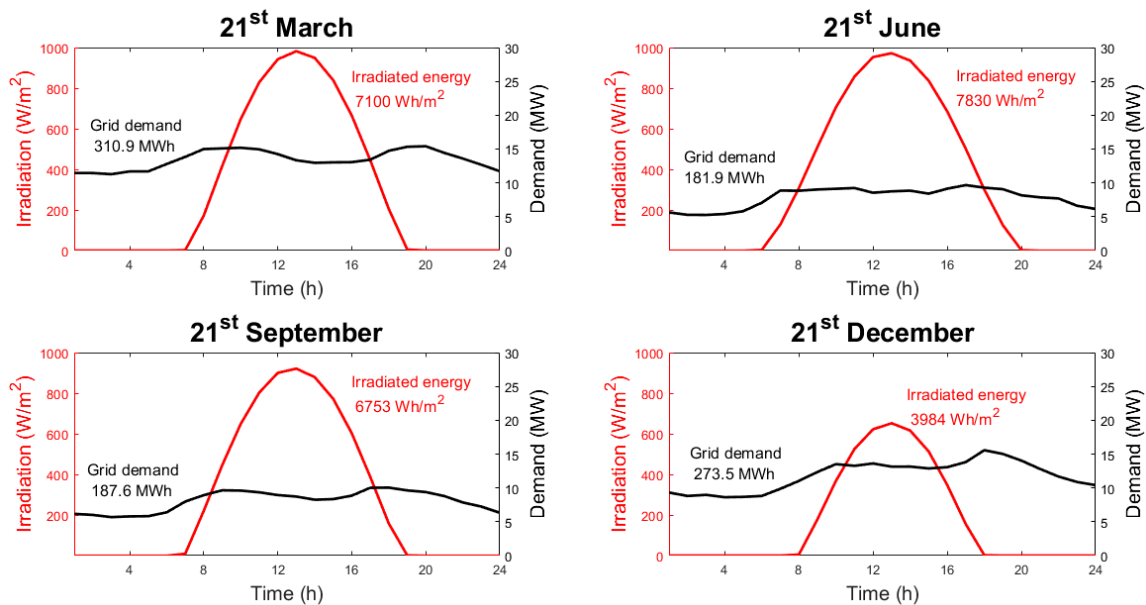
ISCC power plant boundary conditions are shown in Table 1 while components' optimum sizing is a consequence of the flexibility concept needs that are described later. For the topping cycle, the moderate gas turbine inlet temperature has been considered based on the un-fired nature of the ISCC, as other research works suggest [30,32–34]. The relatively low gas turbine inlet temperature implies a low-pressure ratio for the topping cycle and steam generation at the heat recovery steam generator (HRSG). Based on topping cycle operative conditions and molten salts anti-freezing recommendations, molten salts tanks will operate between 265 °C and 430 °C.

Table 1. Power plant layout boundary conditions.

Brayton Cycle		Rankine Cycle		TES Storage Approach	
T <sub>1</sub>	25 °C	T <sub>7</sub>	416.35 °C	T <sub>13</sub>	265 °C
T <sub>3</sub>	850 °C	T <sub>8</sub>	40 °C	T <sub>14</sub>	430 °C
T <sub>5</sub>	265 °C	PHRSG	23 bar		
T <sub>5'</sub>	140 °C				
P <sub>1</sub>	101,300 Pa				
Π	6.5				
η <sub>compressor</sub>	90%	η <sub>pump</sub>	90%		
η <sub>GT</sub>	90%	η <sub>ST</sub>	90%		

As it can be noticed in Figure 2, solar energy harvesting is represented in red as direct normal irradiation, and instantaneous grid demand to be covered (in black) is shifted, which requires an energy storage strategy for mismatch management. In addition,

power variation that is observed throughout the year (both in time and level) implies that the ISCC and storage optimum designs be addressed from an annual perspective. In particular, design criteria to inject the same electricity into the power grid on the 21st of June under both energy approaches have been chosen, as that is the day with the highest solar energy availability.



**Figure 2.** ISCC boundary conditions; grid demand curves (in black) and solar direct normal irradiation (in red) for the plant location.

ISCC plant sizing and its flexible dispatch strategy are designed to maximize the electrical coverage of a microgrid using different energy storage approaches with a great interest for covering the evening peak [10]. Covering that time of the demand would favor ISCC plant concept deployment for its grid balancing role and also allow it to benefit from higher market prices [35]. On the contrary, extending plant production beyond that peak into night hours will result in an oversizing design of both the solar field and storage system that will not be compensated by the lower electrical prices at night [36,37].

#### *Solving Scheme—Flexible Dispatch Strategy*

Figure 3 describes different operation modes of the ISCC plant layout connected to a thermal energy storage system. As it can be observed, in the case of no DNI and an empty hot molten salts tank, the power block does not produce energy. On the contrary, with no DNI but hot salts stored, these are diverted to the HRSG to generate steam in the Rankine cycle to produce the required power so the grid demand can be met. In the case of available DNI, both Brayton and Rankine cycles are connected but working at different loads depending on the grid demand and available storage. In case the available solar energy exceeds grid demand, the surplus energy is diverted for heating and storing molten salts by adjusting the air mass flow ratio that is diverted for steam generation at the HRSG. In this situation, the steam mass flow of the Rankine cycle is instantaneously adapted to meet the grid demand curve. In case the solar energy harvested is not enough to meet grid demand, stored thermal energy from the hot tank is used to supplement the exhaust air from the topping cycle to produce the required steam for meeting grid demand. In those cases, ISCC extended hours of operation will depend on the harvested solar energy, demanded energy from the grid and the thermal stored energy.

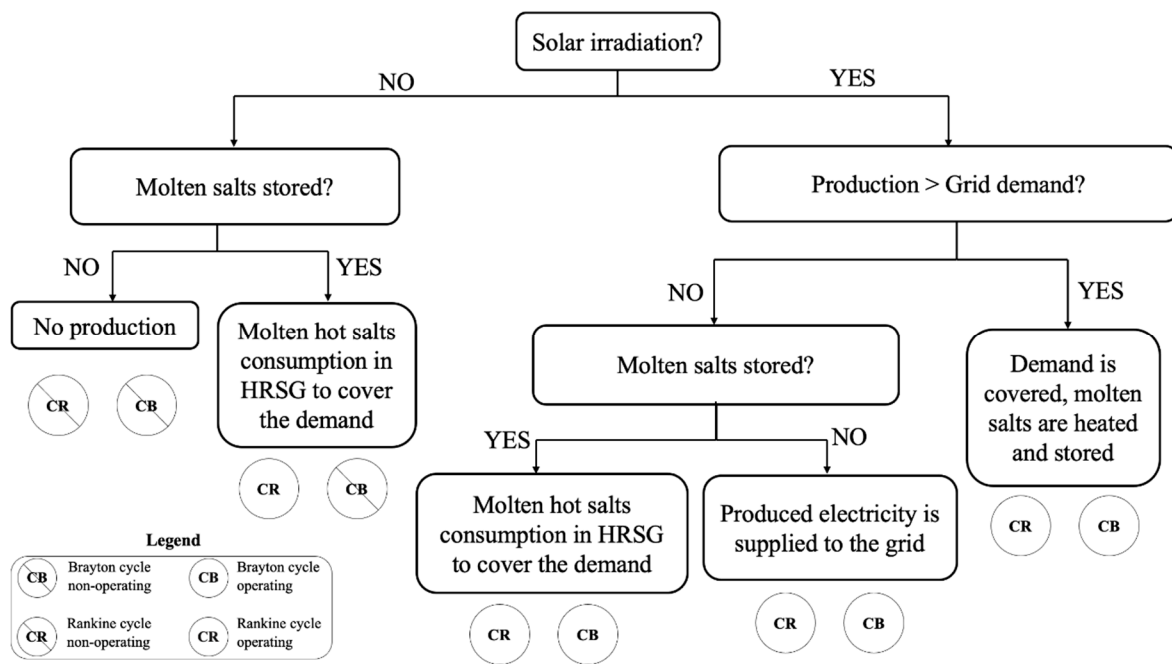


Figure 3. Operational and dispatch flow-chart of the ISCC power plant layout with thermal energy storage (TES) system.

Figure 4 summarizes the different operation modes of the ISCC plant layout when it is connected to the hydrogen production and storage system. As it can be observed, when there is no DNI nor hydrogen stored, the ISCC is out of operation. On the contrary, in the case of having hydrogen stored, it will be consumed at the fuel cell so the grid demand can be met. In the case of solar DNI availability, it is necessary to verify whether plant output production exceeds the instantaneous grid demand or not. Given that plant production is exceeding the grid demand, this can be fully covered, and the electricity surplus would be used for hydrogen production by the electrolysis process. It is important to point out that, unlike Approach A, in this case, the energy surplus is in the form of electricity, which may come with both the Brayton cycle and the Rankine cycle. If the production is lower than the demand, but there is hydrogen stored, this will be consumed so the grid demand can be covered, and if there is no hydrogen stored, the electricity being produced will be supplied to the grid.

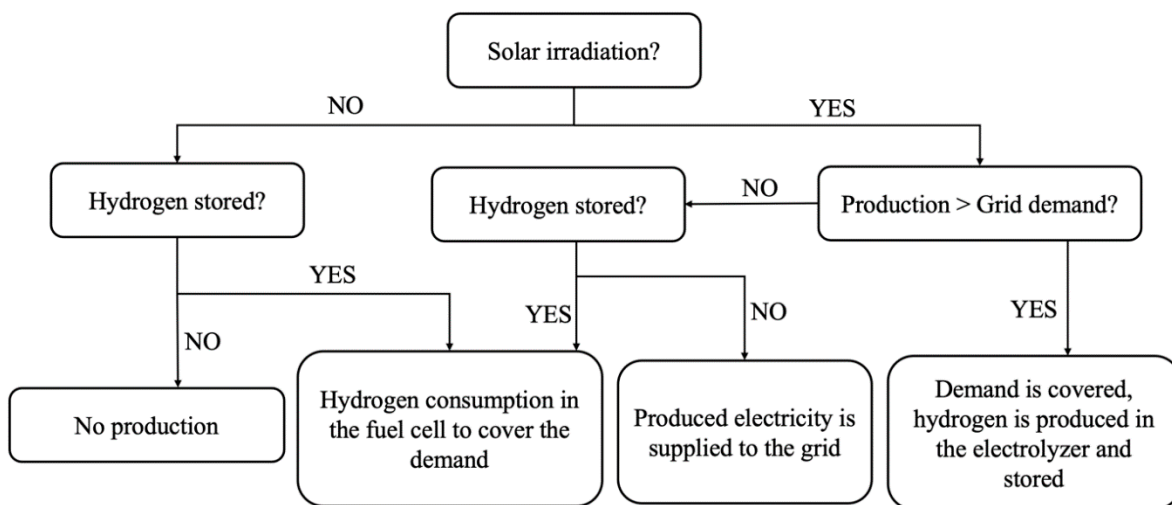


Figure 4. Operational and dispatch flow-chart of the ISCC power plant layout with hydrogen generation system.

In both approaches, plant production is extended until the stored energy is consumed while satisfying grid demand; plant and storage sizing are optimized to allow for evening peak demand coverage.

### 3. Results

Instantaneous operation for both ISCC plant configurations is discussed in this section according to solar energy harvesting, energy production, grid demand and stored energy in the form either of hot molten salts or hydrogen.

#### 3.1. Instantaneous Performance of the Storage Approach A—Molten Salts TES

To clarify the solving scheme presented in Figure 3 and to analyze the relevance of TES integration (Approach A), Figure 5a represents energy surplus availability. As it can be observed, maximum electrical production is constrained by Brayton cycle power as the TES system is fed by gas turbine exhaust energy. Consequently, topping cycle electrical production cannot exceed, at any time, the instantaneous grid demand, which imposes a maximum electrical dispatch of 86.92 MWh based on the user grid demand curve for the 21st of June.

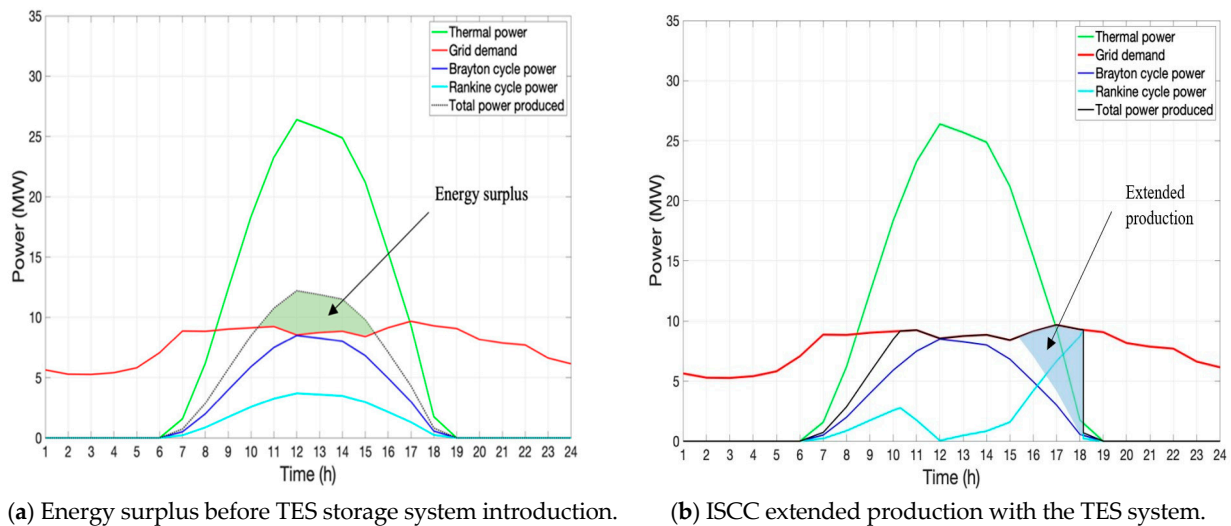


**Figure 5.** Hourly dispatch operation of the ISCC power plant with TES system (21st of June).

According to Figure 5a, the grid demand curve (red series) can be supplied by the combined production of the Brayton topping cycle (dark blue series) and the Rankine bottoming cycle (light blue series). This combined production (dashed black series) can cover grid demand between 10:18 and 15:24, which represents 21.32% of the plant utility factor. As it can be observed, the combined operation of Brayton and Rankine cycles results in an electricity surplus production (shaded area) compared to the requested grid demand. In that event, surplus electricity could not be injected into the grid, which would be translated into missed electrical production. To overcome this situation, active loading of the molten salts thermal energy storage system (Approach A) is proposed and represented in Figure 5b. As it can be noticed, once the TES system is introduced, the Rankine bottoming cycle adapts its production (varying water flow through the HRSG) to the exact electricity required to cover grid demand. In this situation, grid demand can be fully covered between 10:18 and 18:09, which results in a plant utility factor of 32.71%.

As it can be observed in Figure 6, air mass flow within the Brayton cycle follows the same trend as solar DNI based on the ISCC plant layout presented in Figure 1, which implies the online operation of the gas turbine. On the contrary, Rankine cycle water mass flow and its power output can be regulated accordingly so the grid demand can be met. The opposite trend between the air flow diverted to the HRSG (for steam generation) and

the air flow diverted for TES loading can also be noticed. As noted in Figure 5a, energy production exceeded grid demand from 10:18 onwards and thus exhaust air used for steam generation (air to HRSG series) rapidly decreases as most of the exhausted hot air is diverted for TES charging (air to heat salts series). Consequently, water flow in the Rankine cycle is reduced and continuously adapts to satisfy grid demand. From 12:00 onwards, solar radiation slightly decreases (Figure 5) and therefore energy production is supported by the growing contribution of the Rankine cycle. At that point, the exhaust mass flow air diverted for steam generation (air to HRSG series) increases while air diverted for molten salts heating is consequently reduced (air to heat salts series). Accordingly, mass flow through the air–molten salts heat exchanger reduces until 15:24, when the combined operation of Brayton and Rankine cycles are not sufficient for grid demand covering based on the low solar DNI and stored molten salts for extra steam generation (salts to HRSG series). The ISCC plant continues its operation and supplies the required power to meet the demand curve until 18:09, when the hot tank is emptied. As it can be observed from Figure 5b, ISCC with TES approach and the proposed operation scheme can cover the afternoon peak that day, which happened at around 17:00.

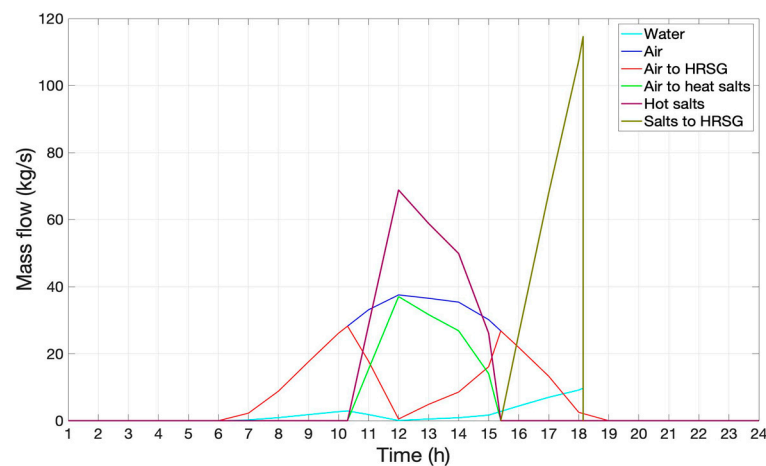
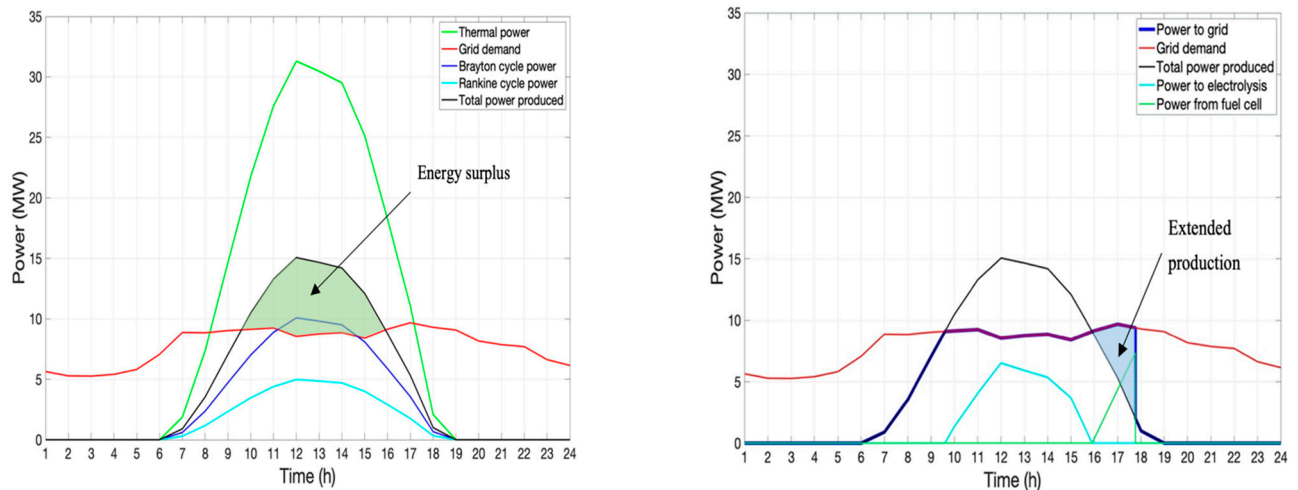


**Figure 6.** Instantaneous mass flow changes for the ISCC power plant with TES system (21st of June).

### 3.2. Storage Approach B—Hydrogen Generation and Storage System

To clarify the solving scheme presented in Figure 4 and to analyze the importance of the hydrogen production strategy (Approach B), Figure 7a represents energy surplus availability. In this situation, there are no limitations in power production from the topping (or bottoming) cycles, as the surplus electricity is diverted for hydrogen production. It must be pointed out that for comparison purposes, the TES and hydrogen storage approaches were sized to inject the same electricity into the grid during the design day.

According to Figure 7a, grid demand can be fully covered from 9:36 to 15:55, as the combined production of the Brayton and Rankine cycles (black series) exceeds the grid demand (red series). In this case, the plant utility factor is 26.32%, which is slightly higher than the corresponding one from Figure 5a based on the larger heliostat field of this configuration. As was advised before, the surplus electricity (shaded area) can be used to run the electrolyzer (light blue series in Figure 7b) to produce hydrogen and store it for later. Once solar energy drastically reduces (from 15:55), there is not enough thermal energy harvested to meet grid demand using the power block of the ISCC. In such a situation, previously generated hydrogen is recovered and used in a fuel cell (light green series) to satisfy the grid demand deficit until all the stored hydrogen is exhausted by 17:46.



(a) Energy surplus before the hydrogen storage system introduction. (b) ISCC extended production with the hydrogen system.

**Figure 7.** Hourly dispatch operation of the ISCC power plant with hydrogen system (21st of June).

It can be observed in Figure 8 that variables linked to the solar DNI (Brayton air and Rankine water circulation) follow the same behavioral trend. As it can be noticed, hydrogen is produced during the period in which production exceeds demand, that is, from 9:36 to 15:55. After that time, hydrogen is quickly depleted to satisfy grid demand by running the fuel cell together with the Brayton and Rankine operations. The maximum power of the fuel cell can be determined as the maximum energy deficit that it has to cover; in this case, 7.34 MW occurring at 17:46. The integration of the hydrogen generation system provides high flexibility to the ISCC plant layout (dark blue series in Figure 7b), as grid demand can be satisfied from 9:36 to 17:46 with no limitation imposed by the Brayton cycle operation. Under this scheme, the plant utility factor increases up to 34.03%.

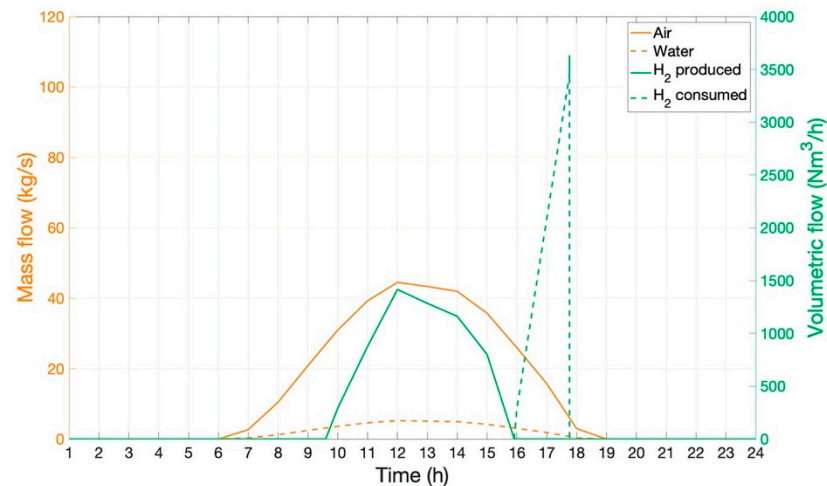


**Figure 8.** Instantaneous mass flow changes for the ISCC power plant with the hydrogen system.

### 3.3. ISCC Plant Components Sizing and Selection

Solar fields from the ISCC power plant under the storage Approach A (molten salts TES) and B (hydrogen production) differ, as shown in Table 2. This is based on the plant operational modes (Figures 2 and 3), different conversion efficiencies of TES and hydrogen generation systems and the selected design criteria for injecting the same electricity into the grid on the 21st of June.

**Table 2.** Heliostat field sizing.

	TES Storage (Approach A)	H <sub>2</sub> Storage (Approach B)
Heliostat field area	54,000 m <sup>2</sup>	64,050 m <sup>2</sup>

Regarding materials selection for the energy storage Approach A, a binary mixture of 60% NaNO<sub>3</sub> and 40% KNO<sub>3</sub> is preferred due to its suitable thermal properties and low chemical reactivity, vapor pressure and cost [38]. Thermophysical properties are gathered in Table 3.

**Table 3.** Binary molten salts properties [39].

Binary Molten Salts: 60% NaNO <sub>3</sub> + 40% KNO <sub>3</sub>	
Hot salts specific heat (at 430 °C)	1.512 kJ/kg °C
Cold salts specific heat (at 265 °C)	1.491 kJ/kg °C
Hot salts density	1836 kg/m <sup>3</sup>
Cold salts density	1912 kg/m <sup>3</sup>
Vapor pressure	<0.01 Pa

In this approach, the storage system consists of two tanks where molten salts are accumulated at different temperature levels; the hot one remains at 430 °C (determined by turbine exhaust temperature) while the cold one stays at 265 °C for freezing prevention [40]. For modeling purposes, both tanks are considered to have the same size, so in case of maintenance or breakdown, the salt mixture can be equally stored in either of them. Based on design day conditions, a charging capacity of 431.59 m<sup>3</sup> is required for the hot tank but an oversizing factor of 125% was considered to incorporate equipment and instrumentation, resulting in a total volume of 539.5 m<sup>3</sup>. An aspect ratio of 1.5 has been considered according to economics and heat loss recommendations [41] what results into 11.56 m for tank height and 7.71 m in diameter.

Regarding materials selection for the energy storage Approach B, hydrogen plant components (electrolyzers, tanks, fuel cells) can be sized based on mass flow values from Figure 8. Currently, the main electrolyzer technologies are proton exchange membrane (PEM), alkaline (AEL) and solid oxide (SOE). Commonly, PEM and AEL electrolyzers operate at moderate temperatures (below 80 °C and 220 °C, respectively), whereas SOE electrolyzers operate at a high temperature (above 600 °C). Predominantly, PEM electrolyzers have a low hydrogen production capacity (below 30 Nm<sup>3</sup>/h) and a moderate efficiency while AEL electrolyzers have a larger production capacity and a higher efficiency [42]. Therefore, an AEL electrolyzer was chosen for this application as it is the most recommended type for large plants connected to the grid. A required production capacity of 1417.39 Nm<sup>3</sup>/h was determined based on the maximum power excess of 6.52 MW registered in Figure 7 and average electrical consumption of alkaline electrolyzers of 4.6 kWh/Nm<sup>3</sup> [43].

Regarding hydrogen storing technologies, storing it as a gas necessitates high-pressure tanks (150–1100 bar), while liquid storage requires cryogenic temperatures based on its low boiling point at ambient conditions (−252.8 °C). Otherwise, hydrogen can be stored chemically, either on solid surfaces (by adsorption), within solids (by absorption) or in the form of chemical/metal hydrides. However, chemical-associated processes take too long and physical storage methods are preferred for large-scale storage applications. Pressurized storage is the most common due to the relative simplicity of the process and its lower energy consumption [44]. Regarding the alternatives for pressurized storage, there are four tank types [45]:

- Type I: Metal pressure vessel (200 bar);
- Type II: Thick metallic liner hoop pressure vessel wrapped with fiber-resin composite (200 bar);

- Type III: Metallic liner pressure vessel fully wrapped with fiber-resin composite (700 bar);
- Type IV: Polymeric liner pressure vessel fully wrapped with fiber-resin composite.

Specifically, for this installation, the storage system does not have to meet stringent requirements in terms of portability, weight or volume, so hydrogen can be stored at 200 bar due to the lower cost. The total energy surplus that corresponds to 6201.77 Nm<sup>3</sup> of hydrogen represents the tanks' volumetric capacity.

As with electrolyzers, there are several fuel cells models: proton exchange membrane (PEMFC), direct methanol (DMFC) and alkaline (AFC) for low-temperature applications; phosphoric acid (PAFC) for medium temperature; and molten carbonate (MCFC) and solid oxide (SOFC) for high temperature. In general terms, MCFC, SOFC and PAFC are used for distributed power generation with considerable power requirements. The other devices (AFC, PEMFC, DMFC) are discarded for ISCC plant layout integration as they are typically used for low-power applications such as portable and mobile generators. SOFC and MCFC are also discarded based on their longer start-up requirements caused by higher operating temperatures. Furthermore, these fuel cells easily degrade, with frequent connection and disconnection operations based on the high-temperature gradient. Considering ISCC plant layout operative conditions, PAFC is the most favorable fuel cell model [46]. On the other hand, considering hydrogen's low heating value (119.93 MJ/kg) and the 42% efficiency of PAFC [43], the chosen fuel cell should supply 25,887 MJ of electrical energy in total. Considering the energy losses of the electrolyzer and fuel cell, the efficiency of the storage unit is reduced to 27.40%.

Table 4 summarizes the working conditions for the different energy storage technologies considered in this simulation work. As it can be noticed, the same electricity injection into the grid was chosen as the design criteria for the design day in both technologies. This results in larger net peak power with hydrogen storage technologies due to the lower components efficiency, which implies a large tank volume design. Operating temperatures of both molten salts storage tanks and hydrogen production systems are provided for comparison purposes.

**Table 4.** Working conditions for the day of design.

	TES Storage (Approach A)	Hydrogen Storage (Approach B)
Net energy for the design day (MWh)	86.92	86.92
Net peak power for design day (MW)	9.67	15.06
GT inlet temperature (°C)	850	850
ST inlet temperature (°C)	416.35	416.35
<b>Storage tank</b>		
Tank type	Fixed Roof	Type I or II
Tank volume	539.5 m <sup>3</sup>	6201.77 Nm <sup>3</sup>
Tank pressure (bar)	1	200
Hot molten salts temperature (°C)	430	-
Cold molten salts temperature (°C)	265	-
<b>Electrolyzer</b>		
Type	-	AEL
Operating temperature (°C)	-	100–150
Pressure (bar)	-	<30
Consumption (kWh/Nm <sup>3</sup> )	-	4.6
Capacity (Nm <sup>3</sup> /h)	-	1417.39
<b>Fuel cell</b>		
Type	-	PAFC
Operating temperature (°C)	-	150–220
Power (MW)	-	7.34
Efficiency (%)	-	42

#### 4. Discussion

In this section, annual performance indicators of the ISCC plant layout operating with the TES system (Approach A) and the hydrogen plant (Approach B) are presented and compared in terms of flexible dispatch and economic analysis.

##### 4.1. Annual Performance

Table 5 gathers the main ISCC annual performance indicators, such as power cycle efficiency, sun-to-electricity efficiency, utility factor, operational hours and energy fluxes. These parameters have been computed taking accumulated energy profiles (as those presented in Section 3.2) throughout the year.

**Table 5.** Annual performance of both ISCC energy storage proposals.

	TES Storage (Approach A)				Hydrogen Storage (Approach B)			
Heliostat area (m <sup>2</sup> )	54,000				64,050			
Combined cycle efficiency (%)	45.21				48.12			
Sun-to-electricity efficiency (%)	20.68				19.09			
Storage unit efficiency (%)	100				27.40			
Utility factor (%)	15.56				24.61			
Total energy harvested (MWh)	126,127.64				150,013.57			
Total electricity produced (MWh)	26,343.42				28,636.57			
Total energy stored (MWh)	2245.87				5234.52			
Daily maximum energy stored (MWh)	12.30				26.28			
Grid demand coverage for each season representative day * (h)	SP	SU	AU	WI	SP	SU	AU	WI
	0	7.85	7.09	0	8.10	8.17	7.36	0
Total demand coverage (h)	1363.28				2155.75			
Storage volume production	78,787.33 (m <sup>3</sup> ) (Heated molten salts)				1,137,978.75 (Nm <sup>3</sup> ) (Hydrogen)			

\* SP: spring, SU: summer, AU: autumn, WI: winter.

As was commented above, a larger heliostat area was required for the hydrogen storage approach as both solutions had to produce the same electricity for the design day and higher energy conversion losses appeared with the hydrogen energy storage system. In addition, maximum electricity production with the TES system (Approach A) was a constraint in the Brayton cycle by grid demand. The higher nominal power for plant Approach B also results in higher annual power cycle conversion efficiency (48.12%), calculated according to Equation (1).

$$\text{Power cycle efficiency (\%)} = \frac{\text{Total electricity produced (MWh)}}{\text{Solar energy absorbed (MWh)}} \times 100 \quad (1)$$

In Approach B, the larger solar energy harvested together with higher storage requirements, both accumulated and on a daily basis, allowed an extended electricity production of 792 extra hours compared to the TES approach. This results in an annual utility factor of 24.61%, calculated according to Equation (2), as the accumulated hours fully cover grid demand compared to the total annual hours.

$$\text{Utility factor (\%)} = \frac{\text{Total coverage (h)}}{8760 \text{ h}} \quad (2)$$

Despite the lower energy harvesting of Approach A, the sun-to-electricity efficiency, calculated according to Equation (3), was slightly higher due to higher energy conversion losses of hydrogen-related components. Obtained values on sun-to-electricity efficiency are comparable to those obtained for similar ISCC power plant proposals [47,48].

$$\text{Sun to electricity efficiency (\%)} = \frac{\text{Total electricity produced (MWh)}}{\text{Total energy harvested (MWh)}} \times 100. \quad (3)$$

Regarding the corresponding volume of the energy stored, heated molten salts volume is considerably lower than that of hydrogen due to their higher energy density.

As it can be noticed, the ISCC power plant was not able to satisfy winter grid demand for TES or hydrogen storage approaches, nor during spring for Approach A. This was due to the fact that the solar plant was sized for the 21st of June when harvested energy was higher (7830 kWh/m<sup>2</sup>) and grid demand was the lowest (181.9 MWh), as shown in Figure 2. The mismatch implies that during days with the highest grid demand (winter and spring) but with the lowest solar availability, the plant was not able to cover grid demand. On the contrary, that design criterion prevented solar field and storage oversizing, as the objective was to cover evening peak demand when possible. In this situation, produced electricity was injected into the grid, although it cannot cover the energy required by the demand. In the case of the hydrogen storage approach, a larger solar field size allowed for spring coverage of the demand.

#### 4.2. Economic Analysis

Apart from the annual energy comparison between both energy storage approaches, it is relevant to shed some light on the energy cost of the novel ISCC plant approaches. Table 6 summarizes the estimated capital expenditures (CAPEX) and operating expenses (OPEX) of both ISCC power plant approaches.

**Table 6.** CAPEX and OPEX estimation for TES storage (Approach A) and hydrogen systems (Approach B).

Direct Capital Costs		TES Storage	H <sub>2</sub> Storage	
Item	Value	Cost (USD, Millions)	Cost (USD, Millions)	Ref.
Gas turbine	235·P <sub>GT</sub> (kW) USD	2.00	1.97	[49]
HRSG	400 USD/kW	4.58	5.01	[50]
Rankine cycle components	8220·P <sub>ST</sub> (kW) <sup>0.7</sup> USD	4.92	3.19	[51]
Tower	156.63 USD/kW	2.78	2.36	[23]
Receiver	97.59 × 10 <sup>3</sup> USD	0.097	0.097	[51]
Solar field	120.48 USD/m <sup>2</sup>	6.51	7.72	[33]
Electrolyzer	1000 USD/kW	-	6.52	[52]
Hydrogen tanks	86 USD/kg	-	0.044	[53]
Fuel cell	2000 USD/kg	-	14.67	[54]
Thermal Storage	21.45 USD/kWh	1.26	-	[55]
<b>Indirect Capital Cost</b>				
Surcharge for construction, engineering and contingencies	10%	2.21	4.36	[23]
<b>Total CAPEX</b>		<b>24.36</b>	<b>48.04</b>	
<b>Yearly Operating Costs</b>				
Solar field	5.4 USD/(m <sup>2</sup> ·year)	0.292	0.346	[56]
Power block	37,954.26 USD/(MW·year)	0.674	0.576	[57]
Thermal Storage	62,400 USD/year	0.625	-	[58]
Electrolyzer	2%—electrolyzer CAPEX	-	0.130	[59]
Hydrogen tanks	1%—tanks CAPEX	-	0.004	[49]
Fuel cell	34 USD/kW	-	0.264	[49]
<b>Total OPEX</b>		<b>1.59</b>	<b>1.31</b>	-

Based on the economic assessment presented in Table 6 and the annual production of the ISCC power plant (Table 5), the levelized cost of electricity (LCoE) is determined according to Equation (4).

$$LCoE \text{ (USD/kWh)} = \frac{fcr \cdot CAPEX(USD) + OPEX(USD)}{\text{Total electricity produced (MWh)} \cdot 1000} \quad (4)$$

where the fixed charge rate (*fcr*) factor depends on the discount rate (*i*), the inflation rate (*P*) and the life expectancy of the plant (*n*).

$$fcr = P + \frac{i \times (1 + i)^n}{(1 + i)^n - 1} \quad (5)$$

As it can be observed in Table 7, LCoE for the ISCC plant with molten salts TES storage system is lower (0.122 USD/kWh) than for hydrogen configuration (0.158 USD/kWh). Even though TES configuration produced less energy on the annual basis due to gas turbine operation constraints (Table 5), its lower CAPEX derived from thermal energy storage components prevailed. On the contrary, higher electricity production with the hydrogen system was not sufficient to reduce the LCoE.

**Table 7.** Levelized cost of electricity (LCoE) for both energy storage approach.

	TES Storage (Approach A)	H <sub>2</sub> Storage (Approach B)
Plant lifetime (years)		30
Inflation rate (%)		0.212
Discount rate (%)		5
LCoE (USD/kWh)	0.122	0.158

Based on the production and economic findings in Tables 5–7, it can be envisioned that further developments in hydrogen system components, such as electrolyzers and fuel cells, will reduce its LCoE estimation. This will be achieved both with higher electricity production as component efficiency increases and due to CAPEX reduction, which in the current study, resulted in twice that of the TES storage approach.

## 5. Conclusions

In this paper, the flexible dispatch operation of an Integrated Solar Combined Cycle (ISCC) was analyzed through two different energy storage approaches to meet grid demand electricity during extended production. The main findings of the paper are as follows:

- Molten salts TES system can be charged using the exceeding exhaust energy from the Brayton turbine during central hours of the day, which enables ISCC online power output regulation to meet users' grid demand.
- Stored molten salts can be used on demand to increase the steam generation and to extend demand coverage when solar incident energy reduces.
- The hydrogen storage system can be charged on demand using the surplus electricity that is produced by the ISCC but not required by users' grid demand.
- Stored hydrogen can be used on demand in a fuel cell to extend demand coverage when solar incident energy reduces.
- According to energy production and economic findings, a 30% reduction in LCoE can be achieved with a molten salts TES storage approach compared to a hydrogen solution based on its lower CAPEX despite the lower energy dispatch. However, greater coverage of the electrical demand can be met with a hydrogen storage approach based on the higher gas turbine generation.

**Author Contributions:** Conceptualization, M.Á.R.-B.; methodology, M.Á.R.-B., A.A.-B., D.C.-B.; software, A.A.-B., D.C.-B.; validation, formal analysis, investigation, data curation, M.Á.R.-B., A.A.-B., D.C.-B.; writing—original draft preparation, M.Á.R.-B.; writing—review and editing, M.Á.R.-B., A.A.-B., D.C.-B.; visualization, A.A.-B., D.C.-B.; supervision, M.Á.R.-B. All authors have read and agreed to the published version of the manuscript.

**Funding:** This research received no external funding.

**Institutional Review Board Statement:** Not applicable.

**Informed Consent Statement:** Not applicable.

**Data Availability Statement:** No new data were created or analyzed in this study. Data sharing is not applicable to this article.

**Conflicts of Interest:** The authors declare no conflict of interest.

## References

1. Jorgenson, A.K.; Alekseyko, A.; Giedraitis, V. Energy consumption, human well-being and economic development in central and eastern European nations: A cautionary tale of sustainability. *Energy Policy* **2014**, *66*, 419–427. [CrossRef]
2. Li, Z.D. An econometric study on China's economy, energy and environment to the year 2030. *Energy Policy* **2003**, *31*, 1137–1150. [CrossRef]
3. Gomez-Echeverri, L. Climate and development: Enhancing impact through stronger linkages in the implementation of the Paris Agreement and the Sustainable Development Goals (SDGs). *Philos. Trans. A* **2018**, *376*. [CrossRef]
4. Murphy, C.; Sun, Y.; Cole, W.; Maclaurin, G.; Turchi, C.; Mehos, M.; Murphy, C.; Sun, Y.; Cole, W.; Maclaurin, G.; et al. *The Potential Role of Concentrating Solar Power within the Context of DOE's 2030 Solar Cost Targets*; National Renewable Energy Lab. (NREL): Golden, CO, USA, 2019; 137p. [CrossRef]
5. Mehos, M.; Turchi, C.; Vidal, J.; Wagner, M.; Ma, Z.; Ho, C.; Kolb, W.; Andraka, C.; Kruiuzenga, A. *Concentrating Solar Power Gen3 Demonstration Roadmap*; Office of Scientific and Technical Information (OSTI): Golden, CO, USA, 2017.
6. Islam, M.; Alam, A.M.S.; Das, C.K. Multi-agent system modeling for managing limited distributed generation of microgrid. In Proceedings of the 2nd International Conference on Electrical Information and Communication Technologies, EICT 2015, Khulna, Bangladesh, 10–12 December 2015; Institute of Electrical and Electronics Engineers Inc.: Manhattan, NY, USA, 2016; pp. 533–538.
7. Patel, K.; Das, N.; Khan, M.M.K. Optimization of hybrid solar, wind and diesel energy systems from economic point of view. In Proceedings of the 2019 29th Australasian Universities Power Engineering Conference, AUPEC 2019, Nadi, Fiji, 26–29 November 2019; Institute of Electrical and Electronics Engineers Inc.: Manhattan, NY, USA, 2019.
8. Ho, C.K.; Iverson, B.D. Review of high-temperature central receiver designs for concentrating solar power. *Renew. Sustain. Energy Rev.* **2014**, *29*, 835–846. [CrossRef]
9. Romero, M.; González-Aguilar, J. Next generation of liquid metal and other high-performance receiver designs for concentrating solar thermal (CST) central tower systems. *Adv. Conc. Sol. Therm. Res. Technol.* **2016**, 129–154. [CrossRef]
10. Zaversky, F.; Les, I.; Sorbet, P.; Sánchez, M.; Valentin, B.; Brau, J.F.; Siros, F. The challenge of solar powered combined cycles—Providing dispatchability and increasing efficiency by integrating the open volumetric air receiver technology. *Energy* **2020**, *194*, 116796. [CrossRef]
11. Reyes-Belmonte, M.A.; Pino, F.J.; Romero, M.; Suarez, C.; González-Aguilar, J.; Guerra, J. Optimization of an integrated solar combined cycle. *AIP Conf. Proc.* **2018**, *2033*, 210012.
12. Ho, C.K. A review of high-temperature particle receivers for concentrating solar power. *Appl. Therm. Eng.* **2016**, *109*, 958–969. [CrossRef]
13. Benoit, H.; Pérez López, I.; Gauthier, D.; Sans, J.-L.; Flamant, G. On-sun demonstration of a 750 °C heat transfer fluid for concentrating solar systems: Dense particle suspension in tube. *Sol. Energy* **2015**, *118*, 622–633. [CrossRef]
14. Lantelme, F.; Groult, H. (Eds.) *Molten Salts Chemistry: From Lab to Applications*; Elsevier: Amsterdam, The Netherlands, 2013; ISBN 978-0-12-398538-5.
15. Crespi, F.; Gavagnin, G.; Sánchez, D.; Martínez, G.S. Supercritical carbon dioxide cycles for power generation: A review. *Appl. Energy* **2017**, *195*, 152–183. [CrossRef]
16. Turchi, C.S.; Ma, Z.; Dyreby, J. Supercritical carbon dioxide power cycle configurations for use in concentrating solar power systems. In Proceedings of the ASME Turbo Expo, Copenhagen, Denmark, 11–15 June 2012; American Society of Mechanical Engineers Digital Collection: New York, NY, USA, 2012; Volume 5, pp. 967–973.
17. Di Maio, D.V.; Boccitto, A.; Caruso, G. Supercritical Carbon Dioxide Applications for Energy Conversion Systems. *Energy Procedia* **2015**, *82*, 819–824. [CrossRef]
18. Reyes-Belmonte, M.A.; Sebastián, A.; Romero, M.; González-Aguilar, J. Optimization of a recompression supercritical carbon dioxide cycle for an innovative central receiver solar power plant. *Energy* **2016**. [CrossRef]
19. SOLARSCO2OL Project. Available online: <https://www.solarsco2ol.eu/> (accessed on 6 April 2021).
20. Scarabeus Project. Available online: <https://www.scarabeusproject.eu/> (accessed on 6 April 2021).
21. Le Moullec, Y.; Qi, Z.; Zhang, J.; Zhou, P.; Yang, Z.; Wang, X.; Chen, W.; Wang, S. Shouhang—EDF 10 MWe Supercritical CO<sub>2</sub> Cycle for CSP Demonstration Project. In Proceedings of the 3rd European Supercritical CO<sub>2</sub> Conference, Paris, France, 19–20 September 2019.
22. Reyes-Belmonte, M.Á. A Bibliometric Study on Integrated Solar Combined Cycles (ISCC), Trends and Future Based on Data Analytics Tools. *Sustainability* **2020**, *12*, 8217. [CrossRef]
23. Rovira, A.; Sánchez, C.; Valdés, M.; Abbas, R.; Barbero, R.; Montes, M.; Muñoz, M.; Muñoz-Antón, J.; Ortega, G.; Varela, F. Comparison of Different Technologies for Integrated Solar Combined Cycles: Analysis of Concentrating Technology and Solar Integration. *Energies* **2018**, *11*, 1064. [CrossRef]
24. Khandelwal, N.; Sharma, M.; Singh, O.; Shukla, A.K. Recent Developments in Integrated Solar Combined Cycle Power Plants. *J. Therm. Sci.* **2020**, *29*, 298–322. [CrossRef]

25. Behar, O.; Khellaf, A.; Mohammedi, K.; Ait-Kaci, S. A review of integrated solar combined cycle system (ISCCS) with a parabolic trough technology. *Renew. Sustain. Energy Rev.* **2014**, *39*, 223–250. [[CrossRef](#)]
26. Mehrpooya, M.; Tosang, E.; Dadak, A. Investigation of a combined cycle power plant coupled with a parabolic trough solar field and high temperature energy storage system. *Energy Convers. Manag.* **2018**, *171*, 1662–1674. [[CrossRef](#)]
27. Hosseini, R.; Soltani, M.; Valizadeh, G. Technical and economic assessment of the integrated solar combined cycle power plants in Iran. *Renew. Energy* **2005**, *30*, 1541–1555. [[CrossRef](#)]
28. Nezammahalleh, H.; Farhadi, F.; Tanhaemami, M. Conceptual design and techno-economic assessment of integrated solar combined cycle system with DSG technology. *Sol. Energy* **2010**, *84*, 1696–1705. [[CrossRef](#)]
29. Kang, Q.; Dewil, R.; Degève, J.; Baeyens, J.; Zhang, H. Energy analysis of a particle suspension solar combined cycle power plant. *Energy Convers. Manag.* **2018**, *163*, 292–303. [[CrossRef](#)]
30. Reyes-Belmonte, M.A.; Romero, M.; González-Aguilar, J. Integrated solar combined cycle using particles as heat transfer fluid and thermal energy storage medium for flexible electricity dispatch. *AIP Conf. Proc.* **2020**, 2303. [[CrossRef](#)]
31. Algieri, A.; Morrone, P.; Rovense, F. Energetic analysis of innovative hybrid biomass/solar organic Rankine cycles (ORCS) for micro-scale CHP applications. In Proceedings of the 25th European Biomass Conference and Exhibition, Stockholm, Sweden, 12–15 June 2017.
32. Siros, F.; Campos, G.F. Optimisation of a low-tit combined cycle gas turbine with application to new generation Solar Thermal Power Plants. In Proceedings of the ASME Turbo Expo, Charlotte, NC, USA, 26–30 June 2017; Volume 3, pp. 1–10. [[CrossRef](#)]
33. Rovense, F.; Reyes-Belmonte, M.A.; González-Aguilar, J.; Amelio, M.; Bova, S.; Romero, M. Flexible electricity dispatch for CSP plant using un-fired closed air Brayton cycle with particles based thermal energy storage system. *Energy* **2019**. [[CrossRef](#)]
34. Rovense, F.; Amelio, M.; Scornaienchi, N.M.; Ferraro, V. Performance analysis of a solar-only gas micro turbine, with mass flow control. *Energy Procedia* **2017**, *126*, 675–682. [[CrossRef](#)]
35. Sioshansi, R.; Denholm, P. The value of concentrating solar power and thermal energy storage. *IEEE Trans. Sustain. Energy* **2010**, *1*, 173–183. [[CrossRef](#)]
36. Schöniger, F.; Thonig, R.; Resch, G.; Lilliestam, J. Making the sun shine at night: Comparing the cost of dispatchable concentrating solar power and photovoltaics with storage. *Energy Sources Part B Econ. Plan. Policy* **2021**, *16*, 55–74. [[CrossRef](#)]
37. Rovense, F.; Reyes-Belmonte, M.A.; González-Aguilar, J.; Amelio, M.; Bova, S.; Romero, M. Application of un-fired closed Brayton cycle with mass flow regulation and particles based thermal energy storage systems for CSP. *AIP Conf. Proc.* **2019**, 2126. [[CrossRef](#)]
38. Serrano-López, R.; Fradera, J.; Cuesta-López, S. Molten salts database for energy applications. *Chem. Eng. Process. Process Intensif.* **2013**, *73*, 87–102. [[CrossRef](#)]
39. Vaka, M.; Walvekar, R.; Jagadish, P.; Khalid, M.; Mubarak, N.M.; Panchal, H. High-temperature molten salts optimisation using mixture design for energy storage application. *J. Energy Storage* **2020**, *32*, 101981. [[CrossRef](#)]
40. Herrmann, U.; Kelly, B.; Price, H. Two-tank molten salt storage for parabolic trough solar power plants. *Energy* **2004**, *29*, 883–893. [[CrossRef](#)]
41. Gao, Y.; He, F.; Xu, T.; Meng, X.; Zhang, M.; Yan, L.; Gao, W. Thermal performance analysis of sensible and latent heat thermal energy storage tanks: A contrastive experiment. *J. Build. Eng.* **2020**, *32*, 101713. [[CrossRef](#)]
42. Gallandat, N.; Romanowicz, K.; Züttel, A. An Analytical Model for the Electrolyser Performance Derived from Materials Parameters. *J. Power Energy Eng.* **2017**, *05*, 34–49. [[CrossRef](#)]
43. Gupta, R.B. *Hydrogen Fuel: Production, Transport, and Storage*; CRC Press: Boca Raton, FL, USA, 2008; ISBN 978-1-4200-4575-8.
44. Olabi, A.G.; Bahar, A.S.; Abdelghafar, A.A.; Baroutaji, A.; Sayed, E.T.; Alami, A.H.; Rezk, H.; Abdelkareem, M.A. Large-vs-scale hydrogen production and storage technologies: Current status and future directions. *Int. J. Hydrogen Energy* **2020**. [[CrossRef](#)]
45. Barral, K.; Barthélémy, H. Hydrogen high pressure tanks storages: Overview and new trends due to H 2 Energy specifications and constraints. *Int. J. Hydrogen Energy* **2011**, *36*, 11056–11067.
46. Larminie, J.; Dicks, A. *Fuel Cell Systems Explained Second Edition*; John Wiley and Sons: Hoboken, NJ, USA, 2003; ISBN 047084857X.
47. Reyes-Belmonte, M.A.; Sebastián, A.; Spelling, J.; Romero, M.; González-Aguilar, J. Annual performance of subcritical Rankine cycle coupled to an innovative particle receiver solar power plant. *Renew. Energy* **2019**, 130. [[CrossRef](#)]
48. Reyes-Belmonte, M.A.; Sebastián, A.; González-Aguilar, J.; Romero, M. Performance comparison of different thermodynamic cycles for an innovative central receiver solar power plant. *AIP Conf. Proc.* **2017**, 1850, 160024.
49. Li, Y.; Xiong, Y. Thermo-economic analysis of a novel cascade integrated solar combined cycle system. *Energy* **2018**, *145*, 116–127. [[CrossRef](#)]
50. Silveira, J.L.; Tuna, C.E. Thermo-economic analysis method for optimization of combined heat and power systems. Part I. *Prog. Energy Combust. Sci.* **2003**, *29*, 479–485. [[CrossRef](#)]
51. Zaversky, F.; Les, I.; Sánchez, M.; Valentin, B.; Brau, J.-F.; Siros, F.; McGuire, J.; Berard, F. Techno-Economic Optimization and Benchmarking of a Solar-Only Powered Combined Cycle with High-Temperature TES Upstream the Gas Turbine. In *Green Energy and Environment*; IntechOpen: London, UK, 2019.
52. IRENA. *Green Hydrogen Cost Reduction Scaling up Electrolysers to Meet the 1.5 °C Climate Goal*; IRENA: Abu Dhabi, United Arab Emirates, 2020.
53. Rivard, E.; Trudeau, M.; Zaghbi, K. Hydrogen storage for mobility: A review. *Materials* **2019**, *12*, 1973. [[CrossRef](#)] [[PubMed](#)]
54. Sveshnikova, A. Estimation of Possibility to Implement Fuel Cell Technology for Decentralized Energy Supply in Russia. Master's Thesis, KTH Royal Institute of Technology, Stockholm, Sweden, 2015.

- 
55. Ma, Z.; Glatzmaier, G.C.; Mehos, M. Development of Solid Particle Thermal Energy Storage for Concentrating Solar Power Plants that Use Fluidized Bed Technology. *Energy Procedia* **2014**, *49*, 898–907. [[CrossRef](#)]
  56. Hamed, O.A.; Kosaka, H.; Bamardouf, K.H.; Al-Shail, K.; Al-Ghamdi, A.S. Concentrating solar power for seawater thermal desalination. *Desalination* **2016**, *396*, 70–78. [[CrossRef](#)]
  57. Sarhosis, V.; Jaya, A.A.; Thomas, H.R. Economic modelling for coal bed methane production and electricity generation from deep virgin coal seams. *Energy* **2016**, *107*, 580–594. [[CrossRef](#)]
  58. Trevisan, S.; Ruan, T.; Wang, W.; Laumert, B. Techno-economic analysis of an innovative purely solar driven combined cycle system based on packed bed TES technology. *AIP Conf. Proc.* **2020**, *2303*. [[CrossRef](#)]
  59. Christensen, A. *Assessment of Hydrogen Production Costs from Electrolysis: United States and Europe*; International Council on Clean Transportation: Washington, DC, USA, 2020; pp. 1–73.